International Journal of
Molecular Sciences

MDPI

Article

Tailoring Silicon Nitride Surface Chemistry for Facilitating Odontogenic Differentiation of Rat Dental Pulp Cells

Yanan Gong [1], Yoshitomo Honda [2,*], Tetsuya Adachi [3], Elia Marin [3,4], Kazushi Yoshikawa [1], Giuseppe Pezzotti [3,4] and Kazuyo Yamamoto [1]

1 Department of Operative Dentistry, Osaka Dental University, 8-1 Kuzuhahanazonocho, Hirakata 573-1121, Japan; gong-y@cc.osaka-dent.ac.jp (Y.G.); kazushi@cc.osaka-dent.ac.jp (K.Y.); yamamoto@cc.osaka-dent.ac.jp (K.Y.)
2 Department of Oral Anatomy, Osaka Dental University, 8-1 Kuzuhahanazonocho, Hirakata 573-1121, Japan
3 Department of Dental Medicine, Graduate School of Medical Science, Kyoto Prefectural University of Medicine, Kajiicho, Kawaramachi-Hirokoji, Kamigyo-ku, Kyoto 602-8566, Japan; t-adachi@koto.kpu-m.ac.jp (T.A.); elia-marin@kit.ac.jp (E.M.); pezzotti@kit.ac.jp (G.P.)
4 Department of Ceramic Physics Laboratory, Kyoto Institute of Technology, Sakyo-ku, Matsugasaki, Kyoto 606-8585, Japan
* Correspondence: honda-y@cc.osaka-dent.ac.jp; Tel.: +81-72-864-3013

Abstract: Silicon nitride (Si_3N_4) can facilitate bone formation; hence, it is used as a biomaterial in orthopedics. Nevertheless, its usability for dentistry is unexplored. The aim of the present study was to investigate the effect of Si_3N_4 granules for the proliferation and odontogenic differentiation of rat dental pulp cells (rDPCs). Four different types of Si_3N_4 granules were prepared, which underwent different treatments to form pristine as-synthesized Si_3N_4, chemically treated Si_3N_4, thermally treated Si_3N_4, and Si_3N_4 sintered with 3 wt.% yttrium oxide (Y_2O_3). rDPCs were cultured on or around the Si_3N_4 granular beds. Compared with the other three types of Si_3N_4 granules, the sintered Si_3N_4 granules significantly promoted cellular attachment, upregulated the expression of odontogenic marker genes (*Dentin Matrix Acidic Phosphoprotein 1* and *Dentin Sialophosphoprotein*) in the early phase, and enhanced the formation of mineralization nodules. Furthermore, the water contact angle of sintered Si_3N_4 was also greatly increased to 40°. These results suggest that the sintering process for Si_3N_4 with Y_2O_3 positively altered the surface properties of pristine as-synthesized Si_3N_4 granules, thereby facilitating the odontogenic differentiation of rDPCs. Thus, the introduction of a sintering treatment for Si_3N_4 granules is likely to facilitate their use in the clinical application of dentistry.

Keywords: dental pulp cells; odontogenic differentiation; silicon nitride; surface wettability; cell adhesion

Citation: Gong, Y.; Honda, Y.; Adachi, T.; Marin, E.; Yoshikawa, K.; Pezzotti, G.; Yamamoto, K. Tailoring Silicon Nitride Surface Chemistry for Facilitating Odontogenic Differentiation of Rat Dental Pulp Cells. *Int. J. Mol. Sci.* **2021**, *22*, 13130. https://doi.org/10.3390/ijms222313130

Academic Editors: Ihtesham Ur Rehman and Thimios A. Mitsiadis

Received: 30 October 2021
Accepted: 1 December 2021
Published: 4 December 2021

1. Introduction

Dental caries are the most prevalent form of chronic disease in both adults and children worldwide [1–3]. Promoting the formation of restorative dentin in decayed areas is thus considered a common clinical treatment method [4]. Pulp tissue contributes to the production of dental hard tissue, including restorative dentin in response to physiological and pathologic stimuli [5,6]. Dental pulp cells are derived from mesenchymal stem cells and have multiple differentiation potential [6,7]; when suitably stimulated, pulp cells can differentiate into odontoblasts and secrete dentin matrix [8–11]. Thus, the vitality of pulp tissue and formation of dentin bridges determine the success of pulp capping treatment [12,13].

Currently, calcium hydroxide is well accepted clinically, owing to its ability to promote the formation of dentin bridges and calcific barriers [14–16]. However, calcium hydroxide does not adhere to dentin and dissolves over time [12], causing the formation of tunnel defects in dentin bridges [17] and leading to the inflammation and necrosis of the pulp tissue [18,19]. Therefore, the development of new pulp-capping agents is essential.

Previous studies have reported that silicon nitride (Si_3N_4) is a non-cytotoxic [20,21] and biocompatible (with the ISO 10993) [22] ceramic material that improves in vitro osteoblast differentiation [20,23] and apatite formation [24]. Si_3N_4 implantation in animal femurs [25,26] was found to promote bone formation around the implant [27,28]. Si_3N_4 implants are FDA-approved and already in clinical use [22,29] as vertebral body fixation implants. The microspectroscopic examinations of a short-term retrieval spinal implant demonstrated that Si_3N_4 possesses a peculiar surface chemistry that greatly accelerates bone repair in vivo [30]. However, the influence of Si_3N_4 on dental pulp cells and its optimal surface conditions remain unexplored to date.

To explore the novel application of Si_3N_4 as a dental material, such as pulp covering material, the aim of the present study was to compare the effects of Si_3N_4 granules with different surface stoichiometries on the viability and odontogenic differentiation of rat dental pulp cells (rDPCs).

2. Results

2.1. Characterization of Si_3N_4 after Different Treatments

Four types of Si_3N_4 granules were prepared: pristine as-synthesized Si_3N_4 (P-Si_3N_4), treated in glacial acetic acidic (A-Si_3N_4), thermally oxidized at 200 °C (T-Si_3N_4), and high-temperature sintered Si_3N_4 (S-Si_3N_4) with the addition of 3 wt.% Y_2O_3 (Table 1).

Table 1. Preparation of silicon nitrides.

Type of Si_3N_4	Abbreviations	Treatment
Pristine-Si_3N_4	P-Si_3N_4	As-synthesized
Acid-Si_3N_4	A-Si_3N_4	Acetic acid, 72 h
Thermal-Si_3N_4	T-Si_3N_4	200 °C, 72 h
Sintered-Si_3N_4	S-Si_3N_4	Sintered at 1600 °C, Y_2O_3 (3 wt.%) added

The macroscopic and Field emission scanning electron microscopic (FE-SEM) images of four different Si_3N_4 powders are shown in Figure 1. The thermal and acid treatment did not cause any noticeable change in the color of the material (Figure 1a). FE-SEM observations at higher magnifications ×10.0 k (Figure 1b) showed that the four powders have a comparable average grain size and similar morphology; they include only a few large particles with a diameter in the order of tens of microns, and a dispersion of smaller micro- and trans-micrometric particles.

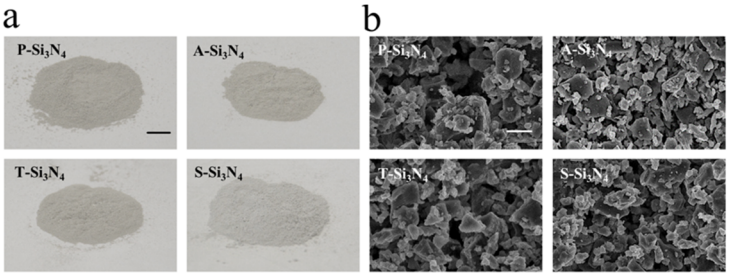

Figure 1. Characterization of Si_3N_4. (**a**) Macroscopic images of Si_3N_4. Scale bar = 5 mm. (**b**) Field emission scanning electron microscopy (FE-SEM) images of Si_3N_4. Scale bar = 10 µm. (P-Si_3N_4: Pristine Si_3N_4, A-Si_3N_4: Acid-treated Si_3N_4, T-Si_3N_4: Thermal-treated Si_3N_4, S-Si_3N_4: Sintered Si_3N_4 with 3 wt.% Y_2O_3).

When investigated by Attenuated total reflection–Fourier transform infrared (ATR-FTIR) spectroscopy (Figure 2a), the four powders produced similar results; the main difference was a peak at 493 cm^{-1}, related to Si-O bonds, which was only visible for the T-Si_3N_4 sample. This result suggests that at the thermal treatment at 200 °C, the

amount and depth of the silica outer layer spontaneously formed on the particles in humid environments [24].

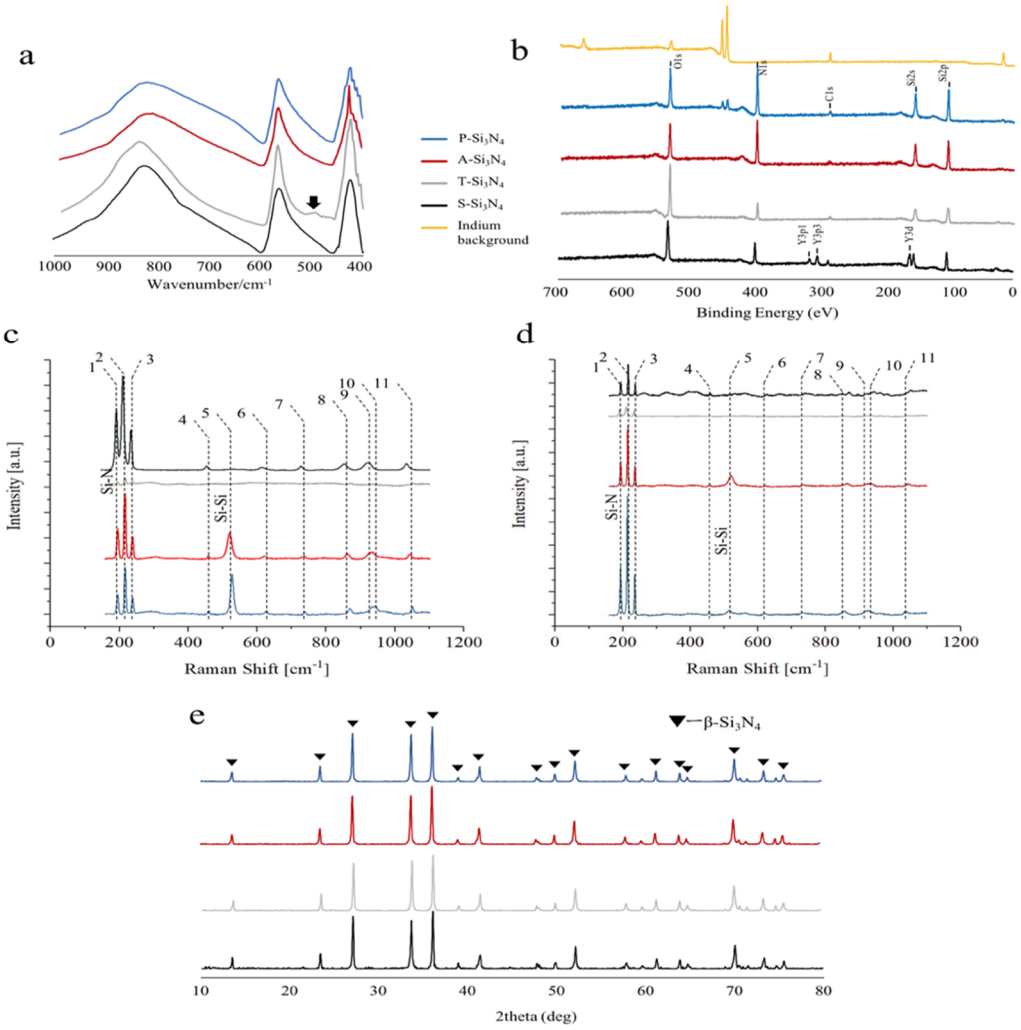

Figure 2. (**a**) Attenuated total reflectance−Fourier transform infrared spectroscopy (ATR−FTIR) spectra of Si_3N_4. Arrows: Si-O bonds. (**b**) X−ray photoelectron spectroscopy (XPS) spectra showing the elements contained in the manufactured Si_3N_4. (**c**) Raman spectroscopy results with green excitation sources. (**d**) Raman spectroscopy results with near infra-red excitation sources. (**e**) X−ray diffraction (XRD) pattern of Si_3N_4 crystals (P-Si_3N_4: Pristine Si_3N_4, A-Si_3N_4: Acid-treated Si_3N_4, T-Si_3N_4: Thermal-treated Si_3N_4, S-Si_3N_4: Sintered Si_3N_4 with 3 wt.% Y_2O_3).

X-ray photoelectron spectroscopy (XPS) analyses (Figure 2b) confirmed the presence of high amounts of oxygen on the T-Si_3N_4 sample when compared to both the A-Si_3N_4 and the P-Si_3N_4 samples. The A-Si_3N_4 showed a surface with a higher content of nitrogen, whereas yttrium, as expected, could only be detected in the S-Si_3N_4 powder sample.

The Raman spectroscopy results with green and near infra-red excitation sources are shown in Figure 2c,d, respectively, whereas the main assignments from band deconvolution are shown in Table 2. The main bands are consistent with the results previously reported in the literature [31], with the exception of a relatively strong band at about 520 cm^{-1} that can be assigned to residual, unreacted amorphous, or micro-crystalline silicon [32]. While the acid post-treatment seems to increase the intensity of the silicon band, the oxidation treatment reduces all band intensities due to the formation of a surface layer of silica, with no active bands in the analyzed spectral window. For the sample containing Y_2O_3, the absence of the Raman band at 520 cm^{-1} suggests a complete reaction during sintering. When compared to the reference spectra (P-Si_3N_4) under green light excitation, the triplet

of bands in the region between 180 and 250 cm^{-1} appear to be broader. This phenomenon was previously associated with the formation of Si–Y–O–N compounds [23] that were speculated to contribute to bone formation in vitro.

Table 2. The main assignments from band deconvolution.

No	Position (Red)	Position (Green)	Assignation	References
1	193	186	E_{2g}	[31]
2	215	210	A_g	[31]
3	235	230	E_{1g}	[31]
4	455	455	E_{2g}	[31]
5	520	520	Si-Si (crystalline)	[32]
6	615	621	E_{2g}	[31]
7	725	730	A_g	[31]
8	855	865	E_{1g}	[31]
9	910	930	E_{2g}	[31]
10	930	945	A_g	[31]
11	1035	1050	E_g	[31]
A	935	960	PO_4^{3-} *v1*	[33]
B	1260	1255	Amide II	[33]
C	1365	1360	D band	[34]
D	-	1680	G band	[34]
E	-	2310	Led light emission	

The powder X-ray diffraction (XRD) patterns of all samples represented the Si_3N_4 β-phase as the predominant phase (Figure 2e). The phase transition evidenced by both ATR-FTIR and XPS could not be detected by XRD, meaning that it was limited to the outer surface of the ceramic particles.

2.2. Characterization of Rat Dental Pulp Cells

The rDPCs were isolated from the mandibular incisor of rats (Figure 3a,b). The expression of cell surface markers CD90, CD34, and CD44 was assessed to identify the cell type of rDPCs. The presence or absence of these markers form the criteria for identifying stem cells. The isolated cells presented a high expression of CD90 and CD44 (the well-known marker of dental pulp stem cells [9,35]) and low expression of CD34 (a primitive hematopoietic progenitor and endothelial cell marker) (Figure 3c), suggesting that the prepared rDPCs are likely heterogeneous cells, including dental pulp stem cells.

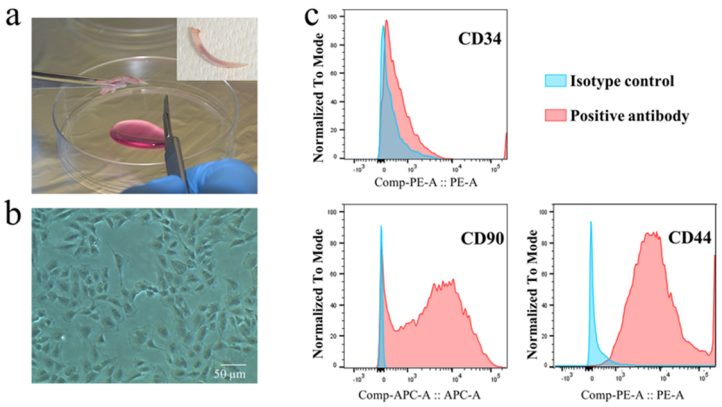

Figure 3. Characterization of primary rat dental pulp cells (rDPCs). (**a**) Mandibular incisors were extracted from rats for isolating rDPCs. (**b**) Microscopic examination showed a fibroblast−like morphology in fourth passage rDPCs. Scale bar = 50 μm. (**c**) Immunophenotype assay by flow cytometric analysis.

2.3. Proliferation of rDPCs Cultured with Si_3N_4

Cell viability on and around the Si_3N_4s was analyzed using wells containing different doses of the ceramics at the center (Figure 4). Fourteen days after cell culture, the total number of cells in the well coated with S-Si_3N_4 showed more significant proliferation compared to that with other Si_3N_4s (Figure 4a). Using live or dead staining at the edge of Si_3N_4 and the polystyrene surface (gray square in Figure 4b), we found that the number of cells on the P-, A-, or T-Si_3N_4 decreased with time compared with that on the polystyrene surface (around Si_3N_4), whereas there was a negligible difference with the cells on the S-Si_3N_4 at day 14 (Figure 4b).

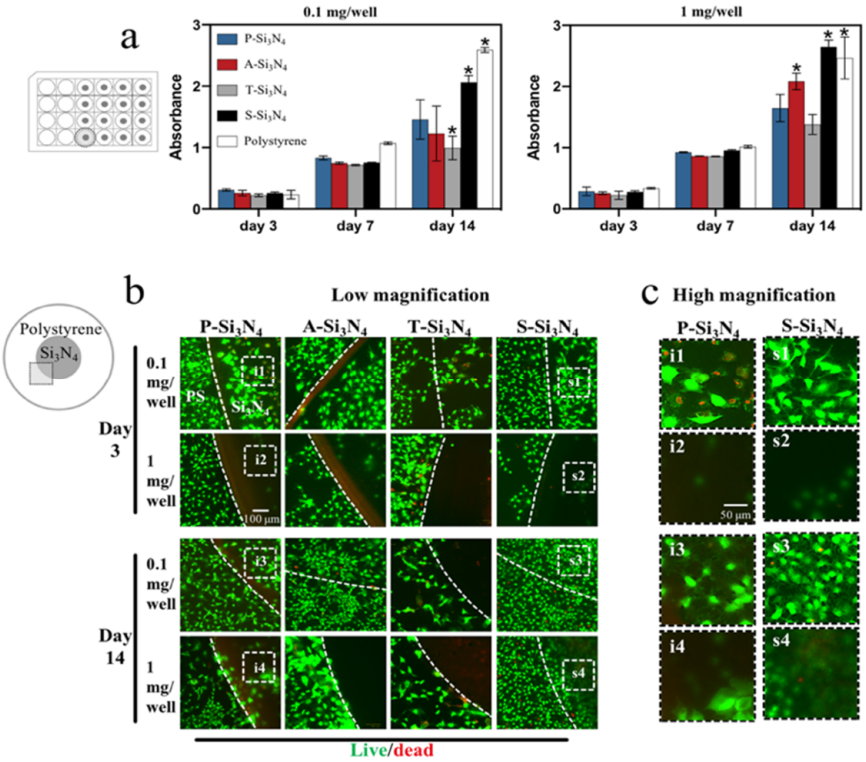

Figure 4. Evaluation of cytotoxicity in vitro. (**a**) Cells incubated with 0.1 and 1 mg/well of Si_3N_4 for different times (3, 7, and 14 days) were analyzed by Cell Counting Kit-8 assay. Data are presented as the mean ± standard deviation (SD) (n = 3). The differences of mean values among the test group were evaluated at one-way analysis of variance and Tukey's multiple comparisons test. * $p < 0.05$: vs. the P-Si_3N_4 group. (**b**) Live/dead viability staining showing the cell activity of the surface with and without Si_3N_4 coating. Green: live cells; red: dead cells. Scale bar = 100 μm. (**c**) High magnification views of P-Si_3N_4 and S-Si_3N_4. Scale bar = 50 μm. (P-Si_3N_4: Pristine Si_3N_4, A-Si_3N_4: Acid-treated Si_3N_4, T-Si_3N_4: Thermal-treated Si_3N_4, S-Si_3N_4: Sintered Si_3N_4 with 3 wt.% Y_2O_3).

2.4. Real-Time Reverse Transcription Quantitative Polymerase Chain Reaction (Real-Time qPCR) Measurement

After treatment with an odontogenic medium, the cells in the S-Si_3N_4-coated wells expressed a higher level of *Dentin Matrix Acidic Phosphoprotein 1* (*DMP-1*) (Figure 5) and *dentin sialophosphoprotein* (*DSPP*) (Supplementary Figure S1) from day three compared to the cells on other Si_3N_4s or on polystyrene.

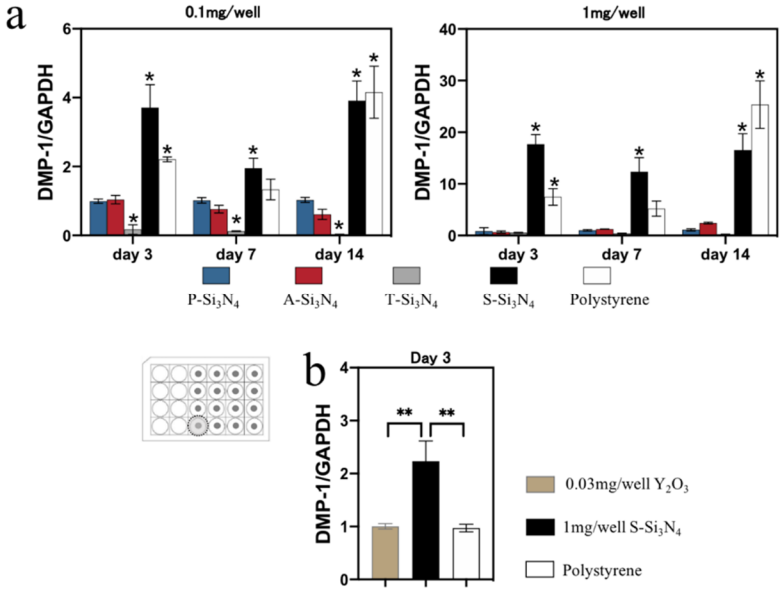

Figure 5. Real-time qPCR to detect the expression of odontoblast-specific genes. (**a**) *Dentin Matrix Acidic Phosphoprotein (DMP-1)* expression at 3, 7, and 14 days on plates coated with P-, A-, T-, S-Si_3N_4. (**b**) *DMP-1* expression at 3 day on plates coated with 1 mg/well of S-Si_3N_4 (3 wt.% Y_2O_3 added) and Y_2O_3 (0.03 mg/well). Data are presented as the mean ± SD (n = 3). The differences of mean values among the test group were evaluated at one-way analysis of variance and Tukey's multiple comparisons test. (**a**) * $p < 0.05$: vs. the P-Si_3N_4 group; (**b**) ** $p < 0.01$: comparison among all groups. (P-Si_3N_4: Pristine Si_3N_4, A-Si_3N_4: Acid-treated Si_3N_4, T-Si_3N_4: Thermal-treated Si_3N_4, S-Si_3N_4: Sintered Si_3N_4 with 3 wt.% Y_2O_3).

2.5. Mineralization Nodules

Mineralized nodule-like structures could be found in the wells with S-Si_3N_4, but not in the wells of other Si_3N_4s except for the 0.1 mg/well A-Si_3N_4 (arrows in Figure 6a). The wells treated with S-Si_3N_4 showed increased alizarin red staining at earlier time points compared to other Si_3N_4-coated wells (Figure 6b,c). Conversely, there was little red staining on and around T-Si_3N_4 subjected with thermal treatment even after 14 days of cell culture, which was weaker than that observed with P-Si_3N_4.

2.6. Raman Characterization

Raman analyses performed after 3 and 14 days of in vitro culture are shown in Figure 7. On day 3, with the exception of S-Si_3N_4 and the positive control, spectra obtained with red light excitation (Figure 7a) showed a prominent silicon band at about 520 cm^{-1}, as previously observed in Figure 2c,d. Two bands related to Si_3N_4 were clearly visible at about 900 cm^{-1}, followed by a shoulder band (A), which was caused by PO_4^{3-} vibrations in bone apatite. At higher Raman shifts, a band related to collagen amide II (B) could be observed, particularly on the P-Si_3N_4 sample, whereas the last band at about 1380 cm^{-1} was derived from the glass substrate. The band at about 1004 cm^{-1} and highlighted in red is related to the presence of phenylalanine and was only visible with the positive control and with the S-Si_3N_4 sample. On day 14 (Figure 7b), the relative intensity of the bands (A) and (B) increased for all samples, particularly for the positive control and for S-Si_3N_4. The phenylalanine signal is barely visible in S-Si_3N_4, but is clearly observed in the positive control.

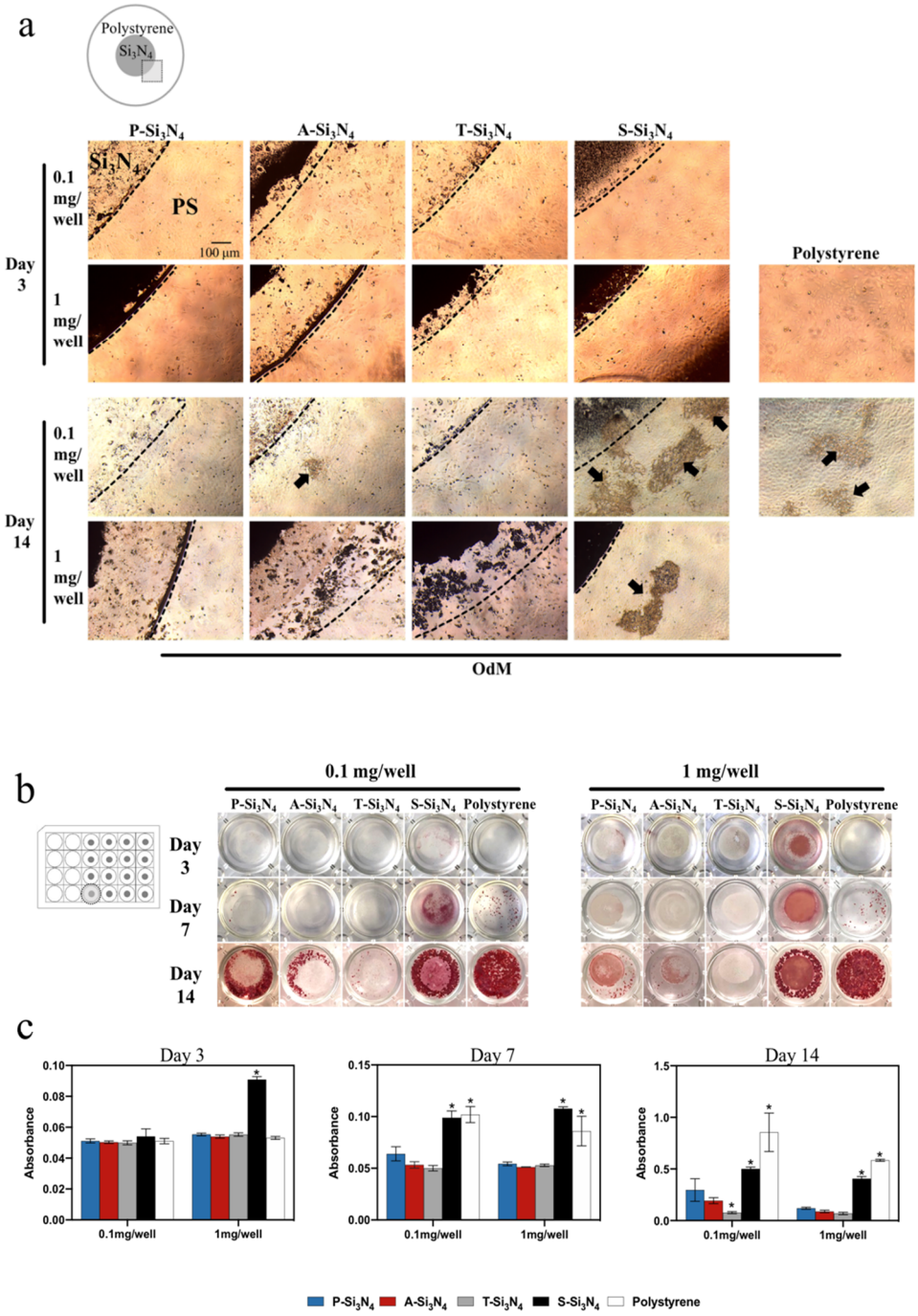

Figure 6. (**a**) Microscopic observation of rDPCs cultured under odontogenic conditions with or without Si_3N_4 for 3 and 14 days. Arrows: Mineralization nodules, Scale bar = 100 μm. (**b**) Effects of Si_3N_4 on calcium deposition examined by alizarin red S staining. (**c**) Histogram of alizarin red S staining quantification. Data are presented as the mean ± SD (n = 3). The differences of mean values among the test group were calculated at one-way analysis of variance and Tukey's multiple comparisons test. * $p < 0.05$: vs. the P-Si_3N_4 group. (P-Si_3N_4: Pristine Si_3N_4, A-Si_3N_4: Acid-treated Si_3N_4, T-Si_3N_4: Thermal-treated Si_3N_4, S-Si_3N_4: Sintered Si_3N_4 with 3 wt.% Y_2O_3, OdM: odontogenic differentiation medium).

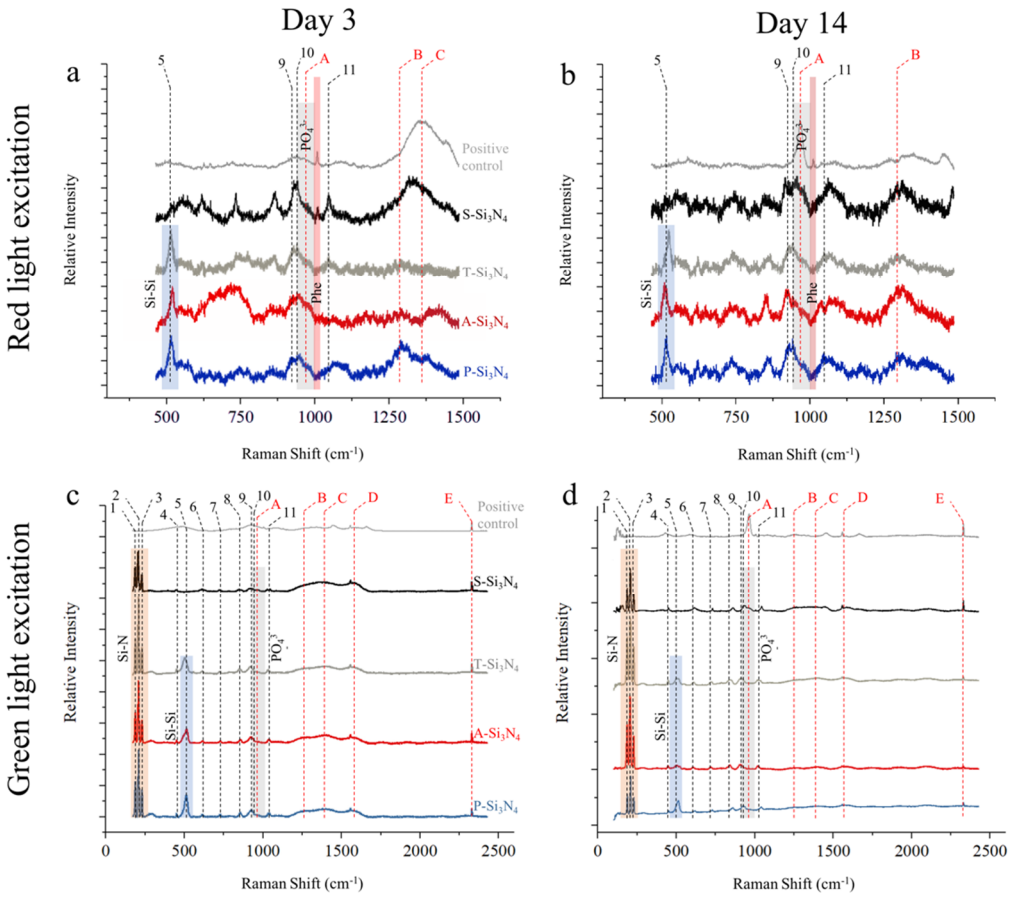

Figure 7. Raman analyses performed after 3 and 14 days of in vitro culture. Raman detection with a red laser after 3 (**a**) or 14 (**b**) days of incubation. Raman detection with a green laser after 3 (**c**) or 14 (**d**) days of incubation. Representative data are presented from three replicate experiments. Numbering and characters are the same as those used in Table 2.

Results obtained under green light excitation are less sensitive to organic material, as confirmed by the spectra obtained after 3 days of in vitro culture (Figure 7c), which strongly resemble those in Figure 2c. The band at about 520 cm^{-1} appears to have a lower relative intensity when compared with the relatively pristine powders, whereas two distinguished bands, (C) and (D), can be attributed to organic matter burning under the power of the laser beam. The results at 14 days (Figure 7d) show the presence of the hydroxyapatite band (A) on both the positive control and the S-Si_3N_4 sample.

2.7. The Effect of Y_2O_3 in S-Si_3N_4 on Odontogenic Differentiation

DMP-1 expression levels of the rDPCs in S-Si_3N_4-coated wells were higher than those cells in wells coated with Y_2O_3 alone (Figure 5b). The cells in both wells showed a different expression pattern.

2.8. Surface Wettability of the Si_3N_4 Surface

The surface wettability of materials strongly affects cell adhesion [36]. The contacts angle of the S-Si_3N_4 surface was significantly higher than that of the surfaces of other Si_3N_4s (Figure 8).

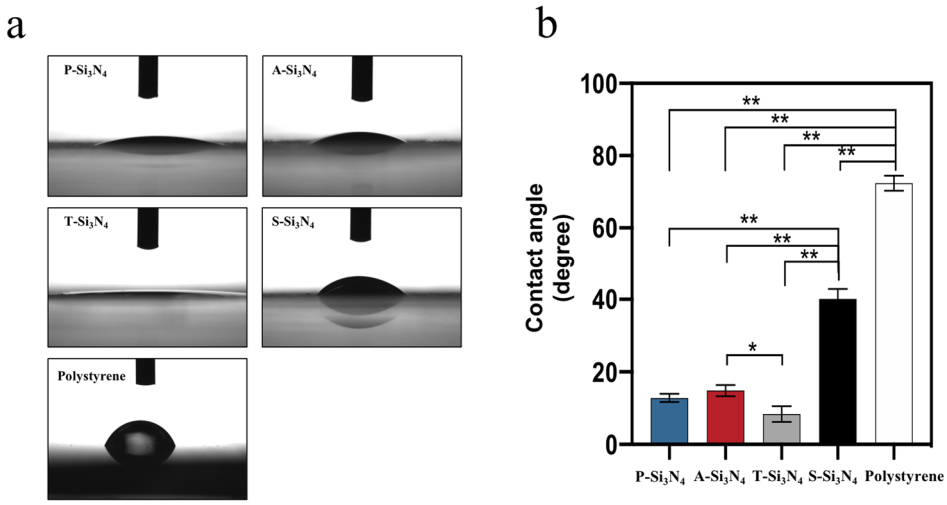

Figure 8. (**a**) Macroscopic images of water absorption at the silicon nitride-coated surface. (**b**) Measurement of the contact angle on the surface of Si_3N_4. Data shown are the means ± SD (n = 3). The differences of mean values among the test groups were evaluated by one-way analysis of variance and Tukey's multiple comparisons test. * $p < 0.05$, ** $p < 0.01$. (P-Si_3N_4: Pristine Si_3N_4, A-Si_3N_4: Acid-treated Si_3N_4, T-Si_3N_4: Thermal-treated Si_3N_4, S-Si_3N_4: Sintered Si_3N_4 with 3 wt.% Y_2O_3).

3. Discussion

Our data show that the Si_3N_4 granules prepared with three different treatments (acid treatment, thermal treatment, and sintered treatment) showed markedly altered surface chemistry compared to the pristine Si_3N_4 granules. The powder bed made of S-Si_3N_4 granules, which underwent a sintering process with the addition of Y_2O_3, showed higher water contact angles compared to the other Si_3N_4s. Coincident with this change, S-Si_3N_4 facilitated the increased proliferation and odontogenic differentiation of rDPCs compared to that with other Si_3N_4s.

Four Si_3N_4s were selectively prepared because of following reasons: the original idea was to compare the as-synthesized (P-Si_3N_4) powder with the sintered (S-Si_3N_4) one; the former being highly pure, was expected to induce the strongest pH buffering effect and thus the highest amount of ammonia eluted, while the latter containing the Y_2O_3 additive as a sintering aid [37] and being thus alloyed by it, was expected to have a milder pH buffering effect and a lower elution of ammonia. Tailoring the pH buffering effect is considered to be key in boosting up cell metabolism without damaging the cells, as ammonia elution beyond a given (unknown so far and different for different types of cells) concentration threshold could be hard for the cells to metabolize. An alternative route to control elution was tried by tuning only the outer surface chemistry: the A-Si_3N_4 sample was treated with acetic acid because there are proofs that treatments in concentrated acetic acid can be used to remove (by esterification) the Si-OH silanol groups that form on the surface of Si_3N_4 [38]. The silanol groups are then restored in aqueous environments, making the surface of the A-Si_3N_4 powders more reactive in the initial stages of hydrolysis; The T-Si_3N_4 sample was obtained by treating the powder at a relatively low temperature (200 °C) in order to produce a thin SiO_2 layer on the outer surface, with the ultimate goal of reducing the reactivity of the powder surface [39] without affecting the bulk of the material.

The expression of *DMP-1* was significantly increased in the early phase of differentiation (day 3 and day 7) in the S-Si_3N_4 group compared to that in the other Si_3N_4s (Figure 5). *DMP-1* expresses during odontogenic differentiation [40]. DMP-1 can nucleate hydroxyapatite formation by binding calcium ions [41]. However, *DMP-1* expression was significantly reduced in mature odontoblasts in vitro [42]. Although we could not elucidate the terminal differentiation of rDPCs due to the limited culture period (14 days), the S-Si_3N_4 granular bed facilitated the early differentiation of rDPCs, suggesting that Si_3N_4 prepared at optimal conditions must have a latent ability to initiate the odontogenic differentiation of rDPCs.

As mentioned above, along with being an early marker of odontogenic differentiation, DMP-1 and DSPP are known to be associated with mineralization [43,44]. Alizarin red staining and Raman spectroscopy are the conventional tools to identify the calcium and phosphate in mineralization [45–47]. In our data, the red staining on S-Si_3N_4 was the strongest compared to that with the other Si_3N_4 groups (Figure 6b). Raman spectroscopy showed significant phosphate spectra on the surface of the S-Si_3N_4 at 960 cm^{-1} (Figure 7). These results support the evidence that DMP-1 and DSPP protein expression, possibly induced by S-Si_3N_4, may partially contribute to early mineralization.

Despite the paucity of information regarding the ability of yttrium to induce odontogenic differentiation, the elements in S-Si_3N_4 were likely to modulate the odontogenic differentiation of rDPCs. However, our data indicate that the expression of *DMP-1* in rDPCs treated with S-Si_3N_4 is inconsistent with that induced by Y_2O_3 alone (Figure 5b), suggesting that odontogenic differentiation induced by S-Si_3N_4 was mainly due to other stimuli rather by yttrium alone, at least for the used doses. The cell adhesion and surface wettability of materials are known to be key regulators of cell differentiation [48,49]. Furthermore, the surface wettability of materials strongly affects cell adhesion [36]. In our results, S-Si_3N_4 showed a higher water contact angle (Figure 8), which was the closest to the optimum angle for cell adhesion [36]. In fact, this finding was consistent with the live or dead staining data in Figure 4b and odontogenic differentiation in Figures 5–7. Based on these results, the sintering process promoted the odontogenic differentiation of rat pulp cells on S-Si_3N_4, partially through the alteration of its surface properties.

Previous studies have evaluated the local and systemic biological response of Si_3N_4 in cell cultures and animal models [25,26]. Si_3N_4 has been shown to be biocompatible in vivo in experiments on sheep [26] and rabbit femurs [25]. Additionally, KUSA-A1 cells [23], SaOS-2 cells [24], and MG63 cells [20] have been found to be effective at in vitro osteogenesis. Most of these findings confer precious insights for bone formation and osteoblastic differentiation, whereas there has been no direct information regarding odontogenic differentiation from pulp cells. To the best of our knowledge, this is the first study using cultured rDPCs isolated from rat dental pulp tissue on and around Si_3N_4 with different surface properties, indicating that Si_3N_4s latently have the ability to alter rDPC activity.

Thermally treated T-Si_3N_4 induced significantly attenuated *DMP-1* expression and mineralized nodule formation compared to that with intact Si_3N_4 (P-Si_3N_4). This observation suggests a role for nitrogen species leaving the surface of Si_3N_4 upon hydrolysis, as suggested previously by one of the authors [50]. Further detailed examination will be necessary to find a better process (concentration, temperature, or additives) for optimizing each Si_3N_4 surface effect in dentistry. For example, it is still unclear whether or not the concurrent presence of Y_2O_3 plays an essential role. In such a case, the optimal sintering temperature or doses of Y_2O_3 remain to be determined. While a complete description of the mechanisms underlying the superior behavior of S-Si_3N_4 in activating rDPCs is missing, the byproducts of hydrolytic reactions of Si_3N_4, such as silanols and nitrogen species including nitride oxide [51], might be associated with the observed proliferation and differentiation of rDPCs. Moreover, the effect of S-Si_3N_4 in dentin formation in vivo remains to be tested. However, our results clearly indicate that different treatments could be effective in altering the surface properties of Si_3N_4 to better increase its bioactivity and to enhance odontogenic differentiation. The present investigation thus provides new insights into the development of novel dental materials based on Si_3N_4 bioceramics.

4. Materials and Methods

4.1. Preparation of Si_3N_4 Granules

Four types of Si_3N_4 granules were prepared: pristine as-synthesized Si_3N_4, treated for 72 h in glacial acetic acidic $\geq$ 99%, thermally oxidized for 72 h at 200 °C, and 1600 °C high-temperature sintered Si_3N_4 with the addition of 3 wt.% Y_2O_3 (Table 1). To ensure the homogeneity of Si_3N_4 granules, these four types of granules were ground separately and

filtered to obtain granules with sizes ranging from 20 to 75 μm, which were then used for the experiments.

4.2. Characterizations of Si_3N_4

FE-SEM images were obtained using the S-4800 FE-SEM system (Hitachi, Tokyo, Japan). All samples were coated with OsO_4 using a Vacuum Device (Ibaraki, Japan). The crystalline phases of Si_3N_4 determined by powder XRD (LabX XRD-6000, SHIMADZU Corporation. Kyoto, Japan), and the chemical structures were characterized by ATR-FTIR spectroscopy (IRAffinity-1S; Shimadzu Corporation, Kyoto, Japan). Chemical composition and chemical bonding were determined by XPS (PHI X-tool; ΦULVAC-PHI, Inc., Kanagawa, Japan) and Raman Spectroscopy (RAMAN touch, Nanophoton, Osaka, Japan).

4.3. Coating of Cell Culture Plates

Two concentrations of Si_3N_4 suspensions were added to the center of 24-well cell culture plates (0.1 and 1 mg/well). After drying at 50 °C for 24 h, the plates were used for cell cultures. All plates were pre-sterilized by exposure to UV light.

4.4. Primary Culture of rDPCs

rDPCs were isolated from the incisor dental pulp tissues of 5-week-old male Wistar-ST rats (Shimizu Laboratory Supplies, Kyoto, Japan). All animal experiments were approved by the Animal Research Committee of Osaka Dental University and performed strictly according to the guidelines (Approval No. 21-02012; approval date: 23 March 2021). The obtained tissues were incubated with collagenase type I (3 mg/mL: Wako Pure Chemical Industries, Osaka, Japan) at 37 °C for 40 min. The fluid containing the cells was centrifuged for 3 min (1000× *g*). The cells were cultured in a Minimum Essential Medium Eagle-Alpha Modification (Nacalai Tesque, Kyoto, Japan), containing 20% fetal bovine serum and 1% penicillin-streptomycin solution (designated as culture medium), at 37 °C in a humidified atmosphere with 5% CO_2. The fourth passage cells were used for this study. To characterize the immunophenotype of rDPCs, the antigen normally expressed on stem cells (APC anti-CD90, PE anti-CD44) and hemopoietic stem cells (PE anti-CD34) were selected. The cells were analyzed by flow cytometry using the FACSVerse™ system (BD, Franklin Lakes, NJ, USA).

4.5. Cell Proliferation Assay

rDPCs were seeded on 24-well plates coated with or without Si_3N_4 (0.1 and 1 mg/well) at 4.0×10^4 cells/well in culture medium. After 3, 7, and 14 days in culture, the Cell Counting Kit-8 (Dojindo Laboratories, Kumamoto, Japan) was used to assess cell proliferation, and absorbance was measured at 450 nm using a plate reader (SpectraMax M5; Molecular Devices, San Jose, CA, USA). The LIVE/DEAD™ Viability/Cytotoxicity Kit was used to assess the state of cellular activity on surfaces with or without Si_3N_4 coating. The results of live/dead fluorescence staining were obtained using the ZOE Fluorescent Cell Imager (Bio-Rad Laboratories, Hercules, CA, USA).

4.6. Real-Time qPCR Assay

rDPCs were cultured in odontogenic differentiation media (OdM), which were prepared by culture medium supplemented with 10 mM glycerol 2-phosphate, 10 (or 100) nM dexamethasone, and 50 (or 155) μM L-ascorbic acid 2-phosphate (FUJIFILM Wako Pure Chemical Corporation, Osaka, Japan). The RNeasy Mini Kit (QIAGEN, Hilden, Germany) was used to extract total RNA from rDPCs. cDNA was synthesized using the SuperScript™ VILO™ cDNA Synthesis Kit (Invitrogen, Thermo Fisher Scientific Inc., Waltham, MA, USA). The mRNA levels of the odontoblast-related DMP-1 and DSPP were investigated using the Step One™ Plus RT-PCR System (ThermoFisher Scientific, Waltham, MA, USA). Glyceraldehyde 3-phosphate dehydrogenase (GAPDH) was regarded as the internal control, and the ΔΔCT method was used for quantifying gene expression. The accession numbers of

the TaqMan gene expression assay PCR system are as follows: DMP-1, Rn01450122_m1; DSPP, Rn02132391_s1; GAPDH, Rn01775763_g1.

4.7. Mineralization Assay

Mineralization nodules were observed by alizarin red S (Sigma-Aldrich, St Louis, MO, USA) staining. rDPCs were cultured in OdM for 3, 7, and 14 days. The medium was aspirated, and the wells were washed with phosphate buffered saline at the respective time points. Cells were fixed with 4% paraformaldehyde, and stained with alizarin red solution for 30 min. To quantify the mineralization nodules, the stain was extracted with 10% formic acid, and the absorbance of the resulting solution was measured at 415 nm using the plate reader (SpectraMax M5).

4.8. Raman Experiment

Each Si_3N_4 or the formation of mineralized nodules on the surface of Si_3N_4 granules were evaluated with a laser Raman microscope (RAMAN touch, Nanophoton, Osaka, Japan) using a 100×.objective lens with a 532.07 nm wavelength green laser and a 785.13 nm wavelength NIR laser. Sample positioning was achieved using a x-y stage controlled with step motors, while an auto-focus function on the Z-axis was used to optimize the signal output. Both the green and NIR laser operated at a nominal power of 200 mW; however, to prevent burning, the power output was reduced by using a neutral-density filter.

At cell culture experiments, cells were cultured on glass plates (MatTek, Ashland, MA, USA) containing 1 mg/well of Si_3N_4 granules for 3 and 14 days using OdM. The group without any Si_3N_4 coating, under the same incubation conditions, was used as the positive control.

4.9. Surface Wettability

The water contact angle of the Si_3N_4-coated surface of the wells was measured separately using contact angle meter LSE-ME (NiCK Corporation, Saitama, Japan) and i2win software.

4.10. Statistical Analysis

Statistical analysis was performed using GraphPad Prism 8 (GraphPad Software Inc., San Diego, CA, USA). All experiments were replicated at least two times. The differences in mean values among the test groups were evaluated using one-way analysis of variance and Tukey's multiple comparisons test. A value of $p < 0.05$ was considered to indicate significant differences.

5. Conclusions

In the present study, we found that sintered granules with the addition of Y_2O_3 possessed altered hydrophilicity compared to pristine as-synthesized Si_3N_4 granules. This resulted in increased pulp cell adhesion, which may promote the odontogenic differentiation of rDPCs in vitro. Conversely, Si_3N_4 granules subjected to thermal treatment at 200 °C in air significantly attenuated the proliferation and differentiation of rDPCs and the formation of mineralized nodules. These results suggest that sintering pre-treatments of Si_3N_4 could be optimized to alter its surface properties, offering an optimal bioactive surface for this bioceramic in dental applications. In summary, this study demonstrates that upon suitable pre-treatment, Si_3N_4 could be considered a novel candidate in the clinical application of dentistry.

Supplementary Materials: The following are available online at https://www.mdpi.com/article/10.3390/ijms222313130/s1.

Author Contributions: Conceptualization Y.H. and G.P.; data curation, Y.G., Y.H., E.M. and G.P.; formal analysis, Y.G. and E.M.; investigation, Y.G. and E.M.; methodology, Y.G., Y.H., E.M. and G.P.; project administration, Y.H.; resources, Y.H. and G.P.; software, Y.G. and E.M.; supervision,

Y.H., G.P. and K.Y. (Kazuyo Yamamoto); validation, Y.G. and E.M.; visualization, Y.G. and E.M.; writing—original draft, Y.G., Y.H., E.M. and G.P.; writing—review and editing, Y.H., T.A., E.M., K.Y. (Kazushi Yoshikawa), G.P. and K.Y. (Kazuyo Yamamoto). All authors have read and agreed to the published version of the manuscript.

Funding: This research received no external funding.

Institutional Review Board Statement: The study was approved by the local ethics committee of Osaka Dental University and strictly adhered to the guidelines (Approval No. 2102012).

Informed Consent Statement: Not applicable.

Data Availability Statement: Not applicable.

Acknowledgments: The authors thank Y. Hashimoto (Department of Biomaterials, Osaka Dental University) and J. Lyu (Department of Orthodontics, Osaka Dental University) for materials used for experiments, N. Kawade (Institute of Dental Research, Osaka Dental University) for technical advice, and H. Liu (Department of Operative Dentistry, Osaka Dental University) for technical support for the experiments.

Conflicts of Interest: The authors declare no conflict of interest.

References

1. Kim, E.S.; Kim, B.I.; Jung, H.I. Age, period and cohort trends in oral health status in South Korean adults. *Community Dent. Oral Epidemiol.* **2021**, *49*, 136–143. [CrossRef]
2. Hu, D.Y.; Hong, X.; Li, X. Oral health in China–trends and challenges. *Int. J. Oral Sci.* **2011**, *3*, 7–12. [CrossRef] [PubMed]
3. Kossioni, A.E. Current status and trends in oral health in community dwelling older adults: A global perspective. *Oral Health Prev. Dent.* **2013**, *11*, 331–340. [CrossRef]
4. Frencken, J.E. Atraumatic restorative treatment and minimal intervention dentistry. *Br. Dent. J.* **2017**, *223*, 183–189. [CrossRef]
5. Stanley, H.R. Pulp capping: Conserving the dental pulp—Can it be done? Is it worth it? *Oral Surg. Oral Med. Oral Pathol.* **1989**, *68*, 628–639. [CrossRef]
6. Sedgley, C.M.; Botero, T.M. Dental stem cells and their sources. *Dent. Clin. N. Am.* **2012**, *56*, 549–561. [CrossRef]
7. Sonoda, S.; Mei, Y.F.; Atsuta, I.; Danjo, A.; Yamaza, H.; Hama, S.; Nishida, K.; Tang, R.; Kyumoto-Nakamura, Y.; Uehara, N.; et al. Exogenous nitric oxide stimulates the odontogenic differentiation of rat dental pulp stem cells. *Sci. Rep.* **2018**, *8*, 3419. [CrossRef]
8. Tziafas, D. Basic mechanisms of cytodifferentiation and dentinogenesis during dental pulp repair. *Int. J. Dev. Biol.* **1995**, *39*, 281–290.
9. Kang, K.J.; Ryu, C.J.; Jang, Y.J. Identification of dentinogenic cell-specific surface antigens in odontoblast-like cells derived from adult dental pulp. *Stem Cell Res. Ther.* **2019**, *10*, 128. [CrossRef]
10. Takeyasu, M.; Nozaki, T.; Watanabe, M.; Shinohara, M.; Morita, J.; Hidaka, A.; Iwamoto, K.; Takahashi, T.; Nagata, S.; Daito, M. In vitro osteogenic differentiation potential of dental pulp stem cells. *J. Oral Tissue Eng.* **2004**, *2*, 25–30.
11. Yokose, S.; Kadokura, H.; Tajima, Y.; Fujieda, K.; Katayama, I.; Matsuoka, T.; Katayama, T. Establishment and characterization of a culture system for enzymatically released rat dental pulp cells. *Calcif. Tissue Int.* **2000**, *66*, 139–144. [CrossRef]
12. Schuurs, A.; Gruythuysen, R.; Wesselink, P. Pulp capping with adhesive resin-based composite vs. calcium hydroxide: A review. *Endod. Dent. Traumatol.* **2000**, *16*, 240–250. [CrossRef] [PubMed]
13. Pameijer, C.H.; Stanley, H.R. The disastrous effects of the "total etch" technique in vital pulp capping in primates. *Am. J. Dent.* **1998**, *11*, S45–S54. [PubMed]
14. Cvek, M. A clinical report on partial pulpotomy and capping with calcium hydroxide in permanent incisors with complicated crown fracture. *J. Endod.* **1978**, *4*, 232–237. [CrossRef]
15. Modena, K.C.D.S.; Casas-Apayco, L.C.; Atta, M.T.; Costa, C.A.d.S.; Hebling, J.; Sipert, C.R.; Navarro, M.F.d.L.; Santos, C.F. Cytotoxicity and biocompatibility of direct and indirect pulp capping materials. *J. Appl. Oral Sci.* **2009**, *17*, 544–554. [CrossRef]
16. Nowicka, A.; Lipski, M.; Parafiniuk, M.; Sporniak-Tutak, K.; Lichota, D.; Kosierkiewicz, A.; Kaczmarek, W.; Buczkowska-Radlinska, J. Response of human dental pulp capped with biodentine and mineral trioxide aggregate. *J. Endod.* **2013**, *39*, 743–747. [CrossRef]
17. Cox, C.; Bergenholtz, G.; Heys, D.; Syed, S.; Fitzgerald, M.; Heys, R. Pulp capping of dental pulp mechanically exposed to oral microflora: A 1–2 year observation of wound healing in the monkey. *J. Oral Pathol. Med.* **1985**, *14*, 156–168. [CrossRef]
18. Cox, C.F.; Sübay, R.K.; Ostro, E.; Suzuki, S.; Suzuki, S.H. Tunnel defects in dentin bridges: Their formation following direct pulp capping. *Oper Dent.* **1996**, *21*, 4–11.
19. Chen, L.; Suh, B.I. Cytotoxicity and biocompatibility of resin-free and resin-modified direct pulp capping materials: A state-of-the-art review. *Dent. Mater. J.* **2017**, *36*, 1–7. [CrossRef]
20. Kue, R.; Sohrabi, A.; Nagle, D.; Frondoza, C.; Hungerford, D. Enhanced proliferation and osteocalcin production by human osteoblast-like MG63 cells on silicon nitride ceramic discs. *Biomaterials* **1999**, *20*, 1195–1201. [CrossRef]

21. Bodišová, K.; Kašiarová, M.; Domanická, M.; Hnatko, M.; Lenčéš, Z.; Nováková, Z.V.; Vojtaššák, J.; Gromošová, S.; Šajgalík, P. Porous silicon nitride ceramics designed for bone substitute applications. *Ceram. Int.* **2013**, *39*, 8355–8362. [CrossRef]
22. Rahaman, M.N.; Yao, A.; Bal, B.S.; Garino, J.P.; Ries, M.D. Ceramics for Prosthetic Hip and Knee Joint Replacement. *J. Am. Ceram. Soc.* **2007**, *90*, 1965–1988. [CrossRef]
23. Pezzotti, G.; Bock, R.M.; Adachi, T.; Rondinella, A.; Boschetto, F.; Zhu, W.; Marin, E.; McEntire, B.; Bal, B.S.; Mazda, O. Silicon nitride surface chemistry: A potent regulator of mesenchymal progenitor cell activity in bone formation. *Appl. Mater. Today* **2017**, *9*, 82–95. [CrossRef]
24. Pezzotti, G.; McEntire, B.J.; Bock, R.; Zhu, W.; Boschetto, F.; Rondinella, A.; Marin, E.; Marunaka, Y.; Adachi, T.; Yamamoto, T.; et al. In Situ Spectroscopic Screening of Osteosarcoma Living Cells on Stoichiometry-Modulated Silicon Nitride Bioceramic Surfaces. *ACS Biomater. Sci. Eng.* **2016**, *2*, 1121–1134. [CrossRef]
25. Howlett, C.R.; McCartney, E.; Ching, W. The effect of silicon nitride ceramic on rabbit skeletal cells and tissue. An in vitro and in vivo investigation. *Clin. Orthop. Relat. Res.* **1989**, *244*, 293–304. [CrossRef]
26. Anderson, M.C.; Olsen, R. Bone ingrowth into porous silicon nitride. *J. Biomed. Mater. Res. A* **2010**, *92*, 1598–1605. [CrossRef]
27. Webster, T.J.; Patel, A.A.; Rahaman, M.N.; Sonny Bal, B. Anti-infective and osteointegration properties of silicon nitride, poly(ether ether ketone), and titanium implants. *Acta Biomater.* **2012**, *8*, 4447–4454. [CrossRef]
28. Ishikawa, M.; de Mesy Bentley, K.L.; McEntire, B.J.; Bal, B.S.; Schwarz, E.M.; Xie, C. Surface topography of silicon nitride affects antimicrobial and osseointegrative properties of tibial implants in a murine model. *J. Biomed. Mater. Res. A* **2017**, *105*, 3413–3421. [CrossRef] [PubMed]
29. Bal, B.S.; Rahaman, M.N. Orthopedic applications of silicon nitride ceramics. *Acta Biomater.* **2012**, *8*, 2889–2898. [CrossRef]
30. Pezzotti, G.; Oba, N.; Zhu, W.; Marin, E.; Rondinella, A.; Boschetto, F.; McEntire, B.; Yamamoto, K.; Bal, B.S. Human osteoblasts grow transitional Si/N apatite in quickly osteointegrated Si_3N_4 cervical insert. *Acta Biomater.* **2017**, *64*, 411–420. [CrossRef]
31. Wada, N.; Solin, S.; Wong, J.; Prochazka, S. Raman and IR absorption spectroscopic studies on α, β, and amorphous Si_3N_4. *J. Non. Cryst. Solids* **1981**, *43*, 7–15. [CrossRef]
32. Smit, C.; Van Swaaij, R.; Donker, H.; Petit, A.; Kessels, W.; Van de Sanden, M. Determining the material structure of microcrystalline silicon from Raman spectra. *J. Appl. Phys.* **2003**, *94*, 3582–3588. [CrossRef]
33. Pezzotti, G.; Rondinella, A.; Marin, E.; Zhu, W.; Aldini, N.N.; Ulian, G.; Valdre, G. Raman spectroscopic investigation on the molecular structure of apatite and collagen in osteoporotic cortical bone. *J. Mech. Behav. Biomed. Mater.* **2017**, *65*, 264–273. [CrossRef] [PubMed]
34. Nakamura, M.; Takagawa, Y.; Miura, K.-i.; Kobata, J.; Zhu, W.; Nishiike, N.; Arao, K.; Marin, E.; Pezzotti, G. Structural alteration induced by substrate bias voltage variation in diamond-like carbon films fabricated by unbalanced magnetron sputtering. *Diam. Relat. Mater.* **2018**, *90*, 214–220. [CrossRef]
35. Bertassoli, B.M.; Costa, E.S.; Sousa, C.A.; Albergaria, J.D.S.; Maltos, K.L.M.; Goes, A.M.; Matins, T.M.d.M.; Silva, G.A.B.; Jorge, E.C. Rat dental pulp stem cells: Isolation and phenotypic characterization method aiming bone tissue bioengineering. *Braz. Arch. Biol. Technol.* **2016**, *59*, e16150613. [CrossRef]
36. Dowling, D.P.; Miller, I.S.; Ardhaoui, M.; Gallagher, W.M. Effect of surface wettability and topography on the adhesion of osteosarcoma cells on plasma-modified polystyrene. *J. Biomater. Appl.* **2011**, *26*, 327–347. [CrossRef]
37. Altun, A.A.; Prochaska, T.; Konegger, T.; Schwentenwein, M. Dense, Strong, and Precise Silicon Nitride-Based Ceramic Parts by Lithography-Based Ceramic Manufacturing. *Appl. Sci.* **2020**, *10*, 996. [CrossRef]
38. Bermudez, V.M. Wet-Chemical Treatment of Si_3N_4 Surfaces Studied Using Infrared Attenuated Total Reflection Spectroscopy. *J. Electrochem. Soc.* **2005**, *152*, F31. [CrossRef]
39. Herrmann, M.; Green, D.J. Corrosion of Silicon Nitride Materials in Aqueous Solutions. *J. Am. Ceram. Soc.* **2013**, *96*, 3009–3022. [CrossRef]
40. Lacerda-Pinheiro, S.; Dimitrova-Nakov, S.; Harichane, Y.; Souyri, M.; Petit-Cocault, L.; Legres, L.; Marchadier, A.; Baudry, A.; Ribes, S.; Goldberg, M.; et al. Concomitant multipotent and unipotent dental pulp progenitors and their respective contribution to mineralised tissue formation. *Eur. Cell Mater.* **2012**, *23*, 371–386. [CrossRef]
41. He, G.; Dahl, T.; Veis, A.; George, A. Nucleation of apatite crystals in vitro by self-assembled dentin matrix protein 1. *Nat. Mater.* **2003**, *2*, 552–558. [CrossRef]
42. D'Souza, R.N.; Cavender, A.; Sunavala, G.; Alvarez, J.; Ohshima, T.; Kulkarni, A.B.; MacDougall, M. Gene expression patterns of murine dentin matrix protein 1 (Dmp1) and dentin sialophosphoprotein (DSPP) suggest distinct developmental functions in vivo. *J. Bone Miner. Res.* **1997**, *12*, 2040–2049. [CrossRef] [PubMed]
43. Narayanan, K.; Ramachandran, A.; Hao, J.; He, G.; Park, K.W.; Cho, M.; George, A. Dual functional roles of dentin matrix protein 1. Implications in biomineralization and gene transcription by activation of intracellular Ca^{2+} store. *J. Biol. Chem.* **2003**, *278*, 17500–17508. [CrossRef] [PubMed]
44. Ching, H.S.; Luddin, N.; Rahman, I.A.; Ponnuraj, K.T. Expression of Odontogenic and Osteogenic Markers in DPSCs and SHED: A Review. *Curr. Stem Cell Res. Ther.* **2017**, *12*, 71–79. [CrossRef] [PubMed]
45. Puchtler, H.; Meloan, S.N.; Terry, M.S. On the history and mechanism of alizarin and alizarin red S stains for calcium. *J. Histochem. Cytochem.* **1969**, *17*, 110–124. [CrossRef]
46. Lievremont, M.; Potus, J.; Guillou, B. Use of alizarin red S for histochemical staining of Ca^{2+} in the mouse; some parameters of the chemical reaction in vitro. *Cells Tissues Organs (Print)* **1982**, *114*, 268–280. [CrossRef]

47. Aljamhan, A.S.; Alrefeai, M.H.; Alhabdan, A.; Alhusseini, S.A.; Farooq, I.; Vohra, F.; Naseem, M.; Alkhudhairy, F. Influence of ER-CR-YSGG Laser and Photodynamic Therapy on the Dentin Bond Integrity of Nano-Hydroxyapatite Containing Resin Dentin Adhesive: SEM-EDX, Micro-Raman, Micro-Tensile, and FTIR Evaluation. *Polymers* **2021**, *13*, 1903. [CrossRef]
48. Ayala, R.; Zhang, C.; Yang, D.; Hwang, Y.; Aung, A.; Shroff, S.S.; Arce, F.T.; Lal, R.; Arya, G.; Varghese, S. Engineering the cell-material interface for controlling stem cell adhesion, migration, and differentiation. *Biomaterials* **2011**, *32*, 3700–3711. [CrossRef]
49. Wang, Y.K.; Chen, C.S. Cell adhesion and mechanical stimulation in the regulation of mesenchymal stem cell differentiation. *J. Cell. Mol. Med.* **2013**, *17*, 823–832. [CrossRef]
50. Pezzotti, G. Silicon Nitride: A Bioceramic with a Gift. *ACS Appl. Mater. Interfaces* **2019**, *11*, 26619–26636. [CrossRef]
51. Pezzotti, G. A spontaneous solid-state NO donor to fight antibiotic resistant bacteria. *Mater. Today Chem.* **2018**, *9*, 80–90. [CrossRef]